

Measurement of Elastic ω Photoproduction at HERA

ZEUS Collaboration

Abstract

The reaction $\gamma p \rightarrow \omega p$ ($\omega \rightarrow \pi^+\pi^-\pi^0$ and $\pi^0 \rightarrow \gamma\gamma$) has been studied in ep interactions using the ZEUS detector at photon-proton centre-of-mass energies between 70 and 90 GeV and $|t| < 0.6 \text{ GeV}^2$, where t is the squared four momentum transferred at the proton vertex. The elastic ω photoproduction cross section has been measured to be $\sigma_{\gamma p \rightarrow \omega p} = 1.21 \pm 0.12 \pm 0.23 \mu\text{b}$. The differential cross section $d\sigma_{\gamma p \rightarrow \omega p}/d|t|$ has an exponential shape $e^{-b|t|}$ with a slope $b = 10.0 \pm 1.2 \pm 1.3 \text{ GeV}^{-2}$. The angular distributions of the decay pions are consistent with s -channel helicity conservation. When compared to low energy data, the features of ω photoproduction as measured at HERA energies are in agreement with those of a soft diffractive process. Previous measurements of the ρ^0 and ϕ photoproduction cross sections at HERA show a similar behaviour.

The ZEUS Collaboration

M. Derrick, D. Krakauer, S. Magill, D. Mikunas, B. Musgrave, J.R. Okrasinski, J. Repond, R. Stanek, R.L. Talaga, H. Zhang

Argonne National Laboratory, Argonne, IL, USA ^p

M.C.K. Mattingly

Andrews University, Berrien Springs, MI, USA

F. Anselmo, P. Antonioli, G. Bari, M. Basile, L. Bellagamba, D. Boscherini, A. Bruni, G. Bruni, P. Bruni, G. Cara Romeo, G. Castellini¹, L. Cifarelli², F. Cindolo, A. Contin, M. Corradi, I. Gialas, P. Giusti, G. Iacobucci, G. Laurenti, G. Levi, A. Margotti, T. Massam, R. Nania, F. Palmonari, A. Pesci, A. Polini, G. Sartorelli, Y. Zamora Garcia³, A. Zichichi

University and INFN Bologna, Bologna, Italy ^f

C. Amelung, A. Bornheim, J. Crittenden, R. Deffner, M. Eckert, L. Feld, A. Frey⁴, M. Geerts⁵, M. Grothe, H. Hartmann, K. Heinloth, L. Heinz, E. Hilger, H.-P. Jakob, U.F. Katz, S. Mengel⁶, E. Paul, M. Pfeiffer, Ch. Rembser, D. Schramm⁷, J. Stamm, R. Wedemeyer

Physikalisches Institut der Universität Bonn, Bonn, Germany ^c

S. Campbell-Robson, A. Cassidy, W.N. Cottingham, N. Dyce, B. Foster, S. George, M.E. Hayes, G.P. Heath, H.F. Heath, D. Piccioni, D.G. Roff, R.J. Tapper, R. Yoshida

H.H. Wills Physics Laboratory, University of Bristol, Bristol, U.K. ^o

M. Arneodo⁸, R. Ayad, M. Capua, A. Garfagnini, L. Iannotti, M. Schioppa, G. Susinno

Calabria University, Physics Dept. and INFN, Cosenza, Italy ^f

A. Caldwell⁹, N. Cartiglia, Z. Jing, W. Liu, J.A. Parsons, S. Ritz¹⁰, F. Sciulli, P.B. Straub, L. Wai¹¹, S. Yang¹², Q. Zhu

Columbia University, Nevis Labs., Irvington on Hudson, N.Y., USA ^q

P. Borzemiński, J. Chwastowski, A. Eskreys, Z. Jakubowski, M.B. Przybycień, M. Zachara, L. Zawiejski

Inst. of Nuclear Physics, Cracow, Poland ^j

L. Adamczyk, B. Bednarek, K. Jeleń, D. Kisiełewska, T. Kowalski, M. Przybycień, E. Rulikowska-Zarebska, L. Suszycki, J. Zając

Faculty of Physics and Nuclear Techniques, Academy of Mining and Metallurgy, Cracow, Poland ^j

Z. Duliński, A. Kotański

Jagellonian Univ., Dept. of Physics, Cracow, Poland ^k

G. Abbiendi¹³, L.A.T. Bauerdick, U. Behrens, H. Beier, J.K. Bienlein, G. Cases, O. Deppe, K. Desler, G. Drews, M. Flasiński¹⁴, D.J. Gilkinson, C. Glasman, P. Göttlicher, J. Große-Knetter, T. Haas, W. Hain, D. Hasell, H. Heßling, Y. Iga, K.F. Johnson¹⁵, P. Joos, M. Kasemann, R. Klanner, W. Koch, U. Kötz, H. Kowalski, J. Labs, A. Ladage, B. Löhner, M. Löwe, D. Lüke, J. Mainusch¹⁶, O. Mańczak, J. Milewski, T. Monteiro¹⁷, J.S.T. Ng, D. Notz, K. Ohrenberg, K. Piotrkowski, M. Roco, M. Rohde, J. Roldán, U. Schneekloth, W. Schulz, F. Selonke, B. Surrow, E. Tassi, T. Voß, D. Westphal, G. Wolf, U. Wollmer, C. Youngman, W. Zeuner

Deutsches Elektronen-Synchrotron DESY, Hamburg, Germany

H.J. Grabosch, S.M. Mari¹⁸, A. Meyer, S. Schlenstedt
DESY-IfH Zeuthen, Zeuthen, Germany

G. Barbagli, E. Gallo, P. Pelfer
University and INFN, Florence, Italy^f

G. Maccarrone, S. De Pasquale, L. Votano
INFN, Laboratori Nazionali di Frascati, Frascati, Italy^f

A. Bamberger, S. Eisenhardt, T. Trefzger¹⁹, S. Wölfle
Fakultät für Physik der Universität Freiburg i.Br., Freiburg i.Br., Germany^c

J.T. Bromley, N.H. Brook, P.J. Bussey, A.T. Doyle, D.H. Saxon, L.E. Sinclair, E. Strickland, M.L. Utey, R. Waugh, A.S. Wilson
Dept. of Physics and Astronomy, University of Glasgow, Glasgow, U.K.^o

A. Dannemann²⁰, U. Holm, D. Horstmann, R. Sinkus²¹, K. Wick
Hamburg University, I. Institute of Exp. Physics, Hamburg, Germany^c

B.D. Burow²², L. Hagge¹⁶, E. Lohrmann, G. Poelz, W. Schott, F. Zetsche
Hamburg University, II. Institute of Exp. Physics, Hamburg, Germany^c

T.C. Bacon, N. Brümmer, I. Butterworth, V.L. Harris, G. Howell, B.H.Y. Hung, L. Lamberti²³, K.R. Long, D.B. Miller, N. Pavel, A. Prinias²⁴, J.K. Sedgbeer, D. Sideris, A.F. Whitfield
Imperial College London, High Energy Nuclear Physics Group, London, U.K.^o

U. Mallik, M.Z. Wang, S.M. Wang, J.T. Wu
University of Iowa, Physics and Astronomy Dept., Iowa City, USA^p

P. Cloth, D. Filges
Forschungszentrum Jülich, Institut für Kernphysik, Jülich, Germany

S.H. An, G.H. Cho, B.J. Ko, S.B. Lee, S.W. Nam, H.S. Park, S.K. Park
Korea University, Seoul, Korea^h

S. Kartik, H.-J. Kim, R.R. McNeil, W. Metcalf, V.K. Nadendla
Louisiana State University, Dept. of Physics and Astronomy, Baton Rouge, LA, USA^p

F. Barreiro, J.P. Fernandez, R. Graciani, J.M. Hernández, L. Hervás, L. Labarga, M. Martinez, J. del Peso, J. Puga, J. Terron, J.F. de Trocóniz
Univer. Autónoma Madrid, Depto de Física Teórica, Madrid, Spain ⁿ

F. Corriveau, D.S. Hanna, J. Hartmann, L.W. Hung, J.N. Lim, C.G. Matthews²⁵, W.N. Murray, A. Ochs, P.M. Patel, M. Riveline, D.G. Stairs, M. St-Laurent, R. Ullmann, G. Zacek²⁵
McGill University, Dept. of Physics, Montréal, Québec, Canada ^{a, b}

T. Tsurugai
Meiji Gakuin University, Faculty of General Education, Yokohama, Japan

V. Bashkirov, B.A. Dolgoshein, A. Stifutkin
Moscow Engineering Physics Institute, Moscow, Russia ^l

G.L. Bashindzhagyan²⁶, P.F. Ermolov, L.K. Gladilin, Yu.A. Golubkov, V.D. Kobrin, I.A. Korzhavina, V.A. Kuzmin, O.Yu. Lukina, A.S. Proskuryakov, A.A. Savin, L.M. Shcheglova, A.N. Solomin, N.P. Zotov
Moscow State University, Institute of Nuclear Physics, Moscow, Russia ^m

M. Botje, F. Chlebana, J. Engelen, M. de Kamps, P. Kooijman, A. Kruse, A. van Sighem, H. Tiecke, W. Verkerke, J. Vossebeld, M. Vreeswijk, L. Wiggers, E. de Wolf, R. van Woudenberg²⁷
NIKHEF and University of Amsterdam, Netherlands ⁱ

D. Acosta, B. Bylsma, L.S. Durkin, J. Gilmore, C.M. Ginsburg, C.L. Kim, C. Li, T.Y. Ling, P. Nylander, I.H. Park, T.A. Romanowski²⁸
Ohio State University, Physics Department, Columbus, Ohio, USA ^p

D.S. Bailey, R.J. Cashmore²⁹, A.M. Cooper-Sarkar, R.C.E. Devenish, N. Harnew, M. Lancaster³⁰, L. Lindemann, J.D. McFall, C. Nath, V.A. Noyes²⁴, A. Quadt, J.R. Tickner, H. Uijterwaal, R. Walczak, D.S. Waters, F.F. Wilson, T. Yip
Department of Physics, University of Oxford, Oxford, U.K. ^o

A. Bertolin, R. Brugnera, R. Carlin, F. Dal Corso, M. De Giorgi, U. Dosselli, S. Limentani, M. Morandin, M. Posocco, L. Stanco, R. Stroili, C. Voci, F. Zuin
Dipartimento di Fisica dell' Università and INFN, Padova, Italy ^f

J. Bulmahn, R.G. Feild³¹, B.Y. Oh, J.J. Whitmore
Pennsylvania State University, Dept. of Physics, University Park, PA, USA ^q

G. D'Agostini, G. Marini, A. Nigro
Dipartimento di Fisica, Univ. 'La Sapienza' and INFN, Rome, Italy ^f

J.C. Hart, N.A. McCubbin, T.P. Shah
Rutherford Appleton Laboratory, Chilton, Didcot, Oxon, U.K. ^o

E. Barberis, T. Dubbs, C. Heusch, M. Van Hook, W. Lockman, J.T. Rahn, H.F.-W. Sadrozinski, A. Seiden, D.C. Williams
University of California, Santa Cruz, CA, USA ^p

J. Biltzinger, R.J. Seifert, O. Schwarzer, A.H. Walenta
Fachbereich Physik der Universität-Gesamthochschule Siegen, Germany^c

H. Abramowicz, G. Briskin, S. Dagan³², T. Doeker³², A. Levy²⁶
*Raymond and Beverly Sackler Faculty of Exact Sciences, School of Physics, Tel-Aviv University,
 Tel-Aviv, Israel*^e

J.I. Fleck³³, M. Inuzuka, T. Ishii, M. Kuze, S. Mine, M. Nakao, I. Suzuki, K. Tokushuku,
 K. Umemori, S. Yamada, Y. Yamazaki
Institute for Nuclear Study, University of Tokyo, Tokyo, Japan^g

M. Chiba, R. Hamatsu, T. Hirose, K. Homma, S. Kitamura³⁴, T. Matsushita, K. Yamauchi
Tokyo Metropolitan University, Dept. of Physics, Tokyo, Japan^g

R. Cirio, M. Costa, M.I. Ferrero, S. Maselli, C. Peroni, R. Sacchi, A. Solano, A. Staiano
Universita di Torino, Dipartimento di Fisica Sperimentale and INFN, Torino, Italy^f

M. Dardo
II Faculty of Sciences, Torino University and INFN - Alessandria, Italy^f

D.C. Bailey, F. Benard, M. Brkic, C.-P. Fagerstroem, G.F. Hartner, K.K. Joo, G.M. Levman, J.F. Martin,
 R.S. Orr, S. Polenz, C.R. Sampson, D. Simmons, R.J. Teuscher
University of Toronto, Dept. of Physics, Toronto, Ont., Canada^a

J.M. Butterworth, C.D. Catterall, T.W. Jones, P.B. Kaziewicz, J.B. Lane, R.L. Saunders, J. Shulman,
 M.R. Sutton
University College London, Physics and Astronomy Dept., London, U.K.^o

B. Lu, L.W. Mo
Virginia Polytechnic Inst. and State University, Physics Dept., Blacksburg, VA, USA^q

W. Bogusz, J. Ciborowski, J. Gajewski, G. Grzelak³⁵, M. Kasprzak, M. Krzyżanowski,
 K. Muchorowski³⁶, R.J. Nowak, J.M. Pawlak, T. Tymieniecka, A.K. Wróblewski, J.A. Zakrzewski,
 A.F. Żarnecki
Warsaw University, Institute of Experimental Physics, Warsaw, Poland^j

M. Adamus
Institute for Nuclear Studies, Warsaw, Poland^j

C. Coldewey, Y. Eisenberg³², D. Hochman, U. Karshon³², D. Revel³², D. Zer-Zion
Weizmann Institute, Nuclear Physics Dept., Rehovot, Israel^d

W.F. Badgett, J. Breitweg, D. Chapin, R. Cross, S. Dasu, C. Foudas, R.J. Loveless, S. Mattingly,
 D.D. Reeder, S. Silverstein, W.H. Smith, A. Vaiciulis, M. Wodarczyk
University of Wisconsin, Dept. of Physics, Madison, WI, USA^p

S. Bhadra, M.L. Cardy³⁷, W.R. Frisken, M. Khakzad, W.B. Schmidke
York University, Dept. of Physics, North York, Ont., Canada^a

¹ also at IROE Florence, Italy
² now at Univ. of Salerno and INFN Napoli, Italy
³ supported by Worldlab, Lausanne, Switzerland
⁴ now at Univ. of California, Santa Cruz
⁵ now a self-employed consultant
⁶ now at VDI-Technologiezentrum Düsseldorf
⁷ now at Commasoft, Bonn
⁸ also at University of Torino and Alexander von Humboldt Fellow
⁹ Alexander von Humboldt Fellow
¹⁰ Alfred P. Sloan Foundation Fellow
¹¹ now at University of Washington, Seattle
¹² now at California Institute of Technology, Los Angeles
¹³ supported by an EC fellowship number ERBFMBICT 950172
¹⁴ now at Inst. of Computer Science, Jagellonian Univ., Cracow
¹⁵ visitor from Florida State University
¹⁶ now at DESY Computer Center
¹⁷ supported by European Community Program PRAXIS XXI
¹⁸ present address: Dipartimento di Fisica, Univ. “La Sapienza”, Rome
¹⁹ now at ATLAS Collaboration, Univ. of Munich
²⁰ now at Star Division Entwicklungs- und Vertriebs-GmbH, Hamburg
²¹ now at Philips Medizin Systeme, Hamburg
²² also supported by NSERC, Canada
²³ supported by an EC fellowship
²⁴ PPARC Post-doctoral Fellow
²⁵ now at Park Medical Systems Inc., Lachine, Canada
²⁶ partially supported by DESY
²⁷ now at Philips Natlab, Eindhoven, NL
²⁸ now at Department of Energy, Washington
²⁹ also at University of Hamburg, Alexander von Humboldt Research Award
³⁰ now at Lawrence Berkeley Laboratory, Berkeley
³¹ now at Yale University, New Haven, CT
³² supported by a MINERVA Fellowship
³³ supported by the Japan Society for the Promotion of Science (JSPS)
³⁴ present address: Tokyo Metropolitan College of Allied Medical Sciences, Tokyo 116, Japan
³⁵ supported by the Polish State Committee for Scientific Research, grant No. 2P03B09308
³⁶ supported by the Polish State Committee for Scientific Research, grant No. 2P03B09208
³⁷ now at TECMAR Incorporated, Toronto

- a* supported by the Natural Sciences and Engineering Research Council of Canada (NSERC)
- b* supported by the FCAR of Québec, Canada
- c* supported by the German Federal Ministry for Education and Science, Research and Technology (BMBF), under contract numbers 057BN19P, 057FR19P, 057HH19P, 057HH29P, 057SI75I
- d* supported by the MINERVA Gesellschaft für Forschung GmbH, the Israel Academy of Science and the U.S.-Israel Binational Science Foundation
- e* supported by the German Israeli Foundation, and by the Israel Academy of Science
- f* supported by the Italian National Institute for Nuclear Physics (INFN)
- g* supported by the Japanese Ministry of Education, Science and Culture (the Monbusho) and its grants for Scientific Research
- h* supported by the Korean Ministry of Education and Korea Science and Engineering Foundation
- i* supported by the Netherlands Foundation for Research on Matter (FOM)
- j* supported by the Polish State Committee for Scientific Research, grants No. 115/E-343/SPUB/P03/109/95, 2P03B 244 08p02, p03, p04 and p05, and the Foundation for Polish-German Collaboration (proj. No. 506/92)
- k* supported by the Polish State Committee for Scientific Research (grant No. 2 P03B 083 08) and Foundation for Polish-German Collaboration
- l* partially supported by the German Federal Ministry for Education and Science, Research and Technology (BMBF)
- m* supported by the German Federal Ministry for Education and Science, Research and Technology (BMBF), and the Fund of Fundamental Research of Russian Ministry of Science and Education and by INTAS-Grant No. 93-63
- n* supported by the Spanish Ministry of Education and Science through funds provided by CICYT
- o* supported by the Particle Physics and Astronomy Research Council
- p* supported by the US Department of Energy
- q* supported by the US National Science Foundation

1 Introduction

Elastic photoproduction of vector mesons, $\gamma p \rightarrow Vp$, has been extensively studied in fixed target experiments at centre-of-mass energies up to $W \approx 20$ GeV. The production of ρ^0 , ω and ϕ is usually described in the framework of the vector meson dominance model (VDM) [1] and Regge theory [2]. The W dependence of the cross section can be parametrised in Regge theory by the sum of two terms, one due to Pomeron exchange and the other to Reggeon exchange. While the latter falls with W , the former is almost flat. Whereas ρ^0 and ϕ production is predominantly due to Pomeron exchange at all energies, the energy behaviour of ω production investigated before HERA suggests a non-negligible contribution from Reggeon exchange. It is therefore of interest to analyse ω photoproduction at HERA, where Pomeron exchange should dominate.

More specifically, it is important to establish if the features typical of elastic ρ^0 and ϕ vector meson production are also observed in ω photoproduction at high energy. Among these features are the weak dependence of the elastic cross section on W , the exponential shape of the differential cross section in t , where t is the squared four momentum transferred at the proton vertex, and s -channel helicity conservation (SCHC). In addition, a comparison of the photoproduction cross sections of the light vector mesons ρ^0 [3, 4], ω and ϕ [5] at HERA energies allows another check of their diffractive production mechanism.

This paper reports a measurement of the photoproduction of ω mesons using the reaction $ep \rightarrow e\omega p$ with the ZEUS detector at HERA. The ω meson is observed via its decay into $\pi^+\pi^-\pi^0$ ($\pi^0 \rightarrow \gamma\gamma$) in the kinematic range $70 < W < 90$ GeV and $p_T^2 < 0.6$ GeV², where p_T is the transverse momentum of the ω with respect to the beam axis. For these events the scattered positron was not observed in the detector, thereby restricting the photon virtuality Q^2 to values smaller than 4 GeV², with a median Q^2 of about 10^{-4} GeV².

2 Kinematics

Elastic ω photoproduction at HERA is measured via the reaction:

$$e(k) + p(P) \rightarrow e(k') + \omega(V) + p(P'),$$

which is shown in Fig. 1. The symbols in brackets denote the four momentum of each particle.

At fixed ep centre-of-mass energy, the inclusive scattering of unpolarized positrons and protons can be described by any pair of the following variables: the four momentum squared carried by the photon,

$$-Q^2 = q^2 = (k - k')^2,$$

the centre-of-mass energy squared of the γ^*p system,

$$W^2 = (q + P)^2 = -Q^2 + 2y(k \cdot P) + M_p^2,$$

where M_p is the proton mass, and the fractional energy transfer of the positron in the proton rest frame,

$$y = (q \cdot P)/(k \cdot P).$$

Additional variables are required to describe elastic vector meson photoproduction: the squared four momentum transferred at the proton vertex,

$$t = (P - P')^2 = (q - V)^2,$$

the angle between the ω production plane and the positron scattering plane, and the polar and azimuthal angles of the normal to the ω decay plane in the s -channel helicity frame.

For the data discussed here, only the decay products of the ω were measured. The value of Q^2 is restricted between the kinematic limit $Q_{min}^2 = M_e^2 \frac{y^2}{1-y} \approx 10^{-9} \text{ GeV}^2$ and $Q_{max}^2 \approx 4 \text{ GeV}^2$, the latter set by the requirement that the scattered positron is not detected in the main detector. At low values of Q^2 the virtual photon is emitted with negligible transverse momentum and with longitudinal momentum $p_{Z\gamma} \approx -E_\gamma$, where E_γ is the photon energy¹. Under these assumptions, t and W can be expressed in terms of the energy E and the longitudinal and transverse momenta p_Z and p_T of the ω in the laboratory frame: $W^2 \approx 2(E - p_Z)E_p$ and $t \approx -p_T^2$, where E_p is the proton beam energy.

In order to determine the photoproduction cross section $\sigma_{\gamma p \rightarrow \omega p}$ from the measured electroproduction cross section $\sigma_{ep \rightarrow e\omega p}$, the following relationship was assumed [5], based on VDM [1] and on the one photon exchange approximation²:

$$\frac{d^2\sigma_{ep \rightarrow e\omega p}}{dydQ^2} = \Phi(y, Q^2) \cdot \sigma_{\gamma p \rightarrow \omega p}(W),$$

¹The ZEUS coordinate system has positive Z in the direction of flight of the beam protons and the X -axis is horizontal, pointing towards the centre of HERA. The nominal interaction point is at $X = Y = Z = 0$.

²The one photon exchange approximation relates the ep cross section to the longitudinal and the transverse γ^*p cross sections for $Q^2 \neq 0$, the latter being related to $\sigma_{\gamma p \rightarrow \omega p}$ by VDM.

where

$$\Phi(y, Q^2) = \frac{\alpha}{2\pi Q^2} \left[\frac{1 + (1 - y)^2}{y} - \frac{2(1 - y)}{y} \left(\frac{Q_{min}^2}{Q^2} - \frac{Q^2}{M_\omega^2} \right) \right] \left(1 + \frac{Q^2}{M_\omega^2} \right)^{-2} \quad (1)$$

is the effective photon flux and $\sigma_{\gamma p \rightarrow \omega p}$ is the photoproduction cross section.

3 Experimental conditions

3.1 HERA

During 1994, HERA operated at a proton energy of 820 GeV and a positron energy of 27.5 GeV. Typically 153 colliding positron-proton bunches were stored, along with 17 unpaired proton and 15 unpaired positron bunches. These additional bunches were used to study background from beam-gas interactions.

3.2 The ZEUS detector

A detailed description of the ZEUS detector can be found elsewhere [6]. In addition to the hadron electron separator, which is described below, the main components used in this analysis are the same as those used for the 1994 ϕ photoproduction analysis [5]. Of the latter, only the calorimeter and the tracking chambers are mentioned here.

Charged particle momenta are reconstructed from information from the vertex detector (VXD) [7], the central tracking detector (CTD) [8] and the rear tracking detector (RTD) [9]. The total angular coverage is $15^\circ < \theta < 170^\circ$, where θ is the polar angle in the ZEUS coordinate system.

The high resolution uranium-scintillator calorimeter (CAL) [10] is divided into three parts, the forward calorimeter (FCAL), the barrel calorimeter (BCAL) and the rear calorimeter (RCAL), respectively covering the polar angle regions 2.6° to 36.7° , 36.7° to 129.1° , and 129.1° to 176.2° . Each part consists of towers which are longitudinally subdivided into electromagnetic (EMC) and hadronic (HAC) readout cells. The transverse sizes are $5 \times 20 \text{ cm}^2$ for the EMC cells ($10 \times 20 \text{ cm}^2$ in the RCAL) and $20 \times 20 \text{ cm}^2$ for the HAC cells. From test beam data, energy resolutions with E in GeV of $\sigma_E/E = 0.18/\sqrt{E}$ for electrons and $\sigma_E/E = 0.35/\sqrt{E}$ for hadrons have been obtained.

The hadron electron separator (HES) [11] consists of silicon detectors $400 \mu\text{m}$ thick. In the 1994 running period only the rear part (RHES) was operational. The RHES

in the RCAL as seen from the interaction point is shown in Figure 2, illustrating the geometrical structure. The RHES is located in the RCAL at a depth of 3.3 radiation lengths, covering an area of about 10 m^2 . Each silicon pad has an area of $28.9 \times 30.5\text{ mm}^2$, providing a spatial resolution of about 9 mm for a single hit pad. If more than one pad is hit by a shower, a cluster consisting of at most 3×3 pads around the most energetic pad is considered. This allows a more precise reconstruction of the position, providing a resolution of about 5 mm for energies greater than 5 GeV. The RHES measures the energy deposited by charged particles near the maximum of an electromagnetic shower. This energy is measured in units m.i.p., the energy deposited by a minimum ionizing particle. The mean energy deposit expected for a shower induced by a 1 GeV photon is 7.6 m.i.p.

3.3 Trigger

The conditions of the three level trigger used in this analysis are those of the 1994 ϕ photoproduction measurement [5].

The requirements at the first trigger level consist of a minimum RCAL electromagnetic energy deposit of 464 MeV reconstructed by the calorimeter trigger processor [12], a maximum deposit of 1250 MeV reconstructed in the FCAL towers surrounding the beam pipe, and at least one track candidate based on CTD information.

Upstream proton-gas interactions are rejected at the second and third trigger levels using calorimeter time measurements.

The third level trigger also uses the CTD information to reject events with a reconstructed vertex more than 66 cm away from the nominal interaction point along Z , with more than four track candidates, or with no pair of tracks forming an invariant mass less than 1.5 GeV assuming the pion mass for each track.

4 Event selection and reconstruction

The data taken during 1994 correspond to a total integrated luminosity of about 3.2 pb^{-1} . After taking the trigger prescaling into account, the data presented in this analysis correspond to an effective integrated luminosity of $894 \pm 13\text{ nb}^{-1}$.

4.1 Selection criteria

The final sample of ω events was selected by imposing the following offline requirements:

- Two tracks with opposite charges associated to a common vertex and no further tracks.
- A well reconstructed π^0 candidate from two clusters (as defined in section 4.2) in RCAL and RHES, with at most one additional cluster, as described in detail below.
- No clusters in BCAL or RCAL with energy greater than 200 MeV and more than 20 cm away from the extrapolated position of either of the two tracks. The cut was not applied to the clusters in the RCAL associated to the π^0 candidate. This cut rejects events with additional neutral particles.
- Transverse momentum of each track greater than 100 MeV and polar angle $\theta \leq 165^\circ$, to restrict the data to a region of good track reconstruction efficiency.
- Total energy in FCAL less than 1 GeV, in order to limit the contamination by proton dissociative events ($\gamma p \rightarrow \omega N$).

4.2 Reconstruction of the π^0

For the reconstruction of the π^0 via the decay photon pair, signals in RCAL and RHES were separately combined into clusters.

RCAL clusters are objects consisting of adjacent calorimeter cells. For the present data, clusters were usually formed by one cell. To reject background from uranium radioactivity, a minimum cell energy of 100 MeV was required. This should be compared with the mean measured photon energy of 500 MeV with a standard deviation of 210 MeV, which is reproduced by the simulations described below.

RHES clusters consist of at most 3×3 adjacent silicon pads (see section 3.2). Most (63%) of the clusters consisted of a single pad. A cut on the signal from any RHES pad with less than 1 m.i.p. was applied to reject noise. The mean RHES signal for this data sample was 4.2 m.i.p. with a standard deviation of 2.5 m.i.p.

RHES clusters were assigned to an RCAL cluster if they were within a distance of 15 cm (measured in the RHES plane). RCAL clusters less than 20 cm away from the extrapolated impact point of a charged track were excluded, thus restricting the

sample to clusters produced by neutral particles. Events with exactly two of these neutral RCAL-RHES clusters were then selected, allowing at most one additional cluster in RCAL with no corresponding RHES cluster and an energy of less than 200 MeV. These two RCAL-RHES clusters were required to have an energy deposition in the electromagnetic part of the calorimeter only. Fewer than 0.5% of the RCAL clusters were associated with more than one RHES cluster. Even less frequent were events in which the two decay photons were assigned to one RHES cluster.

Using the Monte Carlo simulations described in section 5, the energy of the RCAL clusters was corrected for losses in the material between the interaction point and the RCAL. The corrected RCAL energies and RHES position information were used to calculate the two-cluster invariant mass $M_{\gamma\gamma}$. The spectrum is plotted in Fig. 3(a). A fit with the sum of a Gaussian and a second order polynomial yields a mean of the Gaussian of $\langle M_{\gamma\gamma} \rangle = 124 \pm 1$ MeV and a standard deviation of 28 ± 1 MeV. The difference with respect to the π^0 mass is a consequence of the incomplete description of low energy electromagnetic showers in the Monte Carlo simulation. Events with $84 < M_{\gamma\gamma} < 164$ MeV, i.e. a mass within 1.5σ of $\langle M_{\gamma\gamma} \rangle$, were selected.

To improve the resolution in the four momentum and invariant mass of the $\pi^+\pi^-\pi^0$ system, the invariant mass of the two photons was constrained to the π^0 mass. Since the π^0 energies are small, only large opening angles α between the decay photons occur. As the angle α is well determined due to the precise position measurement of RHES, the resolution in $M_{\gamma\gamma}$ is dominated by the energy resolution of RCAL. Thus only the energies were modified in the procedure. The modified values $E_{1_{fit}}, E_{2_{fit}}$ of the corrected energies E_1, E_2 of the RCAL clusters were determined by minimizing the quantity:

$$\chi^2(E_{1_{fit}}, E_{2_{fit}}) = \frac{(E_1 - E_{1_{fit}})^2}{\sigma_{E_1}^2} + \frac{(E_2 - E_{2_{fit}})^2}{\sigma_{E_2}^2}, \quad (2)$$

using the constraint:

$$\sqrt{2 \cdot E_{1_{fit}} E_{2_{fit}} \cdot (1 - \cos \alpha)} = M_{\pi^0},$$

where $\sigma_{E_i}(\text{GeV}) \propto \sqrt{E_i(\text{GeV})}$ are the corresponding energy resolutions of the RCAL.

4.3 Reconstruction of the ω

To determine the invariant mass of the $\pi^+\pi^-\pi^0$ system and the relevant kinematical quantities, the four momentum $p_{3\pi}$ of the $\pi^+\pi^-\pi^0$ system was obtained by adding up

the momenta of the two tracks, assuming pion masses, and the momentum of the π^0 . The latter was determined from the measured RHES positions and the fitted RCAL energies $E_{1_{fit}}$ and $E_{2_{fit}}$. The quantities W and p_T were then derived from $p_{3\pi}$.

The analysis was restricted to the range $70 < W < 90$ GeV, where the acceptance is almost flat. Furthermore the region $p_T^2 < 0.6$ GeV² was selected, to limit the background contamination due to proton dissociation.

5 Acceptance calculation and Monte Carlo simulation

The Monte Carlo generators PYTHIA [13] and DIPSI [14] were used to evaluate the acceptance. The former simulates the γp interaction based on VDM and Regge theory, while the Q^2 spectrum is generated using the ALLM parametrisation [15] of the ep cross section. The latter uses a model by Ryskin [16], describing vector meson production in terms of a fluctuation of the photon into a $q\bar{q}$ pair, which interacts with the proton via a pomeron exchange. The effective W dependence of the γp cross section for the events generated was of the type $\sigma \propto W^{0.2}$. Neither model contains initial or final state radiation. The effect of radiative corrections on the cross section has been estimated to be smaller than 4% [3].

The events were generated in the kinematic range $60 \leq W \leq 100$ GeV and $Q_{min}^2 \leq Q^2 \leq 4$ GeV². In order to adjust the Monte Carlo calculation to the data, the differential cross section $d\sigma/d|t|$ (see section 7.3) was calculated using the default parameters of PYTHIA and the Monte Carlo events were then re-weighted with the measured slope parameter. The angular distribution of the decay pions was assumed to be that implied by SCHC. The reconstructed W , p_T^2 and decay angular distributions of the Monte Carlo sample agree well with those of the data, as do the RCAL and RHES energy distributions of the decay photons.

The RCAL trigger efficiency was determined using the data rather than a Monte Carlo simulation. To this purpose a sample of charged pions from the decay of ρ^0 mesons produced in elastic photoproduction was used. Since one of the two pions is sufficient to trigger the event, the efficiency for RCAL to trigger on a charged pion was evaluated as the fraction of events in which the second pion could have satisfied the trigger and in which it actually did. The uncertainty in the resulting RCAL trigger efficiency is limited by statistics and is 6%. The contribution of the photons from the π^0 decay to the RCAL trigger decision was determined using the Monte Carlo

events described above. The total acceptance of the trigger is about 30%. The largest contribution to the inefficiency is the RCAL energy threshold (about 50%).

The acceptance as a function of W and p_T^2 is shown in Figure 4. The drop of the acceptance with increasing W or with decreasing p_T^2 is due to one or more of the ω decay products escaping detection in the rear region close to the beam pipe. Conversely, with decreasing W the energy of the photons from the π^0 decay falls below the value of the cut on the calorimeter energy, thus decreasing the acceptance.

The acceptance evaluated with PYTHIA was used for the cross section determination. The average acceptance in the region $70 < W < 90$ GeV is 0.89%. It is dominated by the π^0 reconstruction, which has itself an efficiency of 8%. The efficiency is further reduced by the trigger, the requirement of two tracks (55%) and the other offline requirements (about 70%). The model dependence of the acceptance determination was estimated by changing the distributions of W , t and the ω decay angles in the Monte Carlo simulation within the statistical uncertainties allowed by the data.

The PYTHIA Monte Carlo sample shows agreement between the reconstructed and generated values of W and p_T^2 . The relative resolution in W is 6% and the resolution in p_T^2 is better than 0.04 GeV^2 . They are both dominated by the resolution in the energy measurement of the π^0 decay photons.

A determination of the elastic cross section for $\gamma p \rightarrow \phi p$ using the decay $\phi \rightarrow \pi^+\pi^-\pi^0$ was used as a consistency check (see section 7.2). Also in this case the acceptance was determined using PYTHIA. SCHC was assumed and the events were weighted according to the measured t distribution for this reaction [5]. The average acceptance in the region $70 < W < 90$ GeV is 1.5%.

6 Background

Three sources of background were studied. The first is due to inelastic reactions with dissociation of the photon into a system of large mass. The efficiency for detecting an ω meson appearing in the final state of these processes is 10^{-5} . Therefore the contribution of this background to the resonance is negligible. It contributes only to the background below the ω peak, which is discussed in section 7.1.

The main source of background is the inelastic reaction $\gamma p \rightarrow \omega N$, where N is a hadronic system produced by the dissociation of the proton. This background was statistically removed using the results of [3], based on a Monte Carlo simulation with a cross section of the form $d^2\sigma/dtdM_N^2 \propto e^{-b|t|}/M_N^\beta$ (M_N being the mass of the state

N), with $b = 4.5 \text{ GeV}^{-2}$ and $\beta = 2.5$. In [3] the fraction of elastic ρ^0 events was determined as a function of p_T^2 . A similar determination using the present data was not possible due to statistical limitations. The same fraction of elastic events was therefore assumed here and a p_T^2 dependent weight applied to each event to obtain the elastic ω cross section. The overall effect is to lower the cross section by $16 \pm 9\%$. The relative uncertainty on the correction was assumed to be the same as in [3]. The correction was extrapolated to $p_T^2 = 0.6 \text{ GeV}^2$ from the range of the measurement presented in [3].

Contamination from interactions of the proton or positron beam with the residual gas in the beam pipe was estimated from the unpaired bunches to be below 2%.

7 Results

7.1 Analysis of the mass spectrum

The spectrum of the invariant mass of the $\pi^+\pi^-\pi^0$ system $M_{3\pi}$, after all offline cuts and the fit constraining the $\gamma\gamma$ mass according to equation (2), is shown in Figure 3(b). In addition to the ω signal, a second one is visible, which is due to the elastic photoproduction of the ϕ meson, $\gamma p \rightarrow \phi p (\phi \rightarrow \pi^+\pi^-\pi^0)$. The spectrum was fitted with the function:

$$f(M_{3\pi}) = g_1(M_{3\pi}) + g_2(M_{3\pi}) + \zeta(M_{3\pi}), \quad (3)$$

where g_1 , g_2 are convolutions of a non-relativistic Breit-Wigner function with a Gaussian to describe the ω and ϕ resonances. ζ is a third order polynomial representing the background, mainly due to contamination under the π^0 peak and to inelastic processes in which a π^0 is produced. The fitted values of the ω and ϕ masses are $778 \pm 3 \text{ MeV}$ and $1020 \pm 9 \text{ MeV}$, respectively, compatible with those of the Particle Data Group (PDG) [17] and with Monte Carlo expectations. The fitted values of the Gaussian standard deviations are $32 \pm 4 \text{ MeV}$ and $26 \pm 11 \text{ MeV}$, respectively, also in accord with the Monte Carlo; they are a measure of the resolution of the apparatus.

The number of ω and ϕ candidates observed after background subtraction was determined by integrating the fitted Breit-Wigner functions within the kinematic limits. This yields $N_\omega = 172 \pm 17$ and $N_\phi = 38 \pm 15$.

7.2 Elastic $\gamma p \rightarrow \omega p$ cross section

The elastic $\gamma p \rightarrow \omega p$ cross section is given by:

$$\sigma_{\gamma p \rightarrow \omega p} = \frac{N_\omega}{\epsilon \Phi \mathcal{L} B},$$

where N_ω is the total number of observed events after the statistical subtraction of the inelastic background, ϵ is the total acceptance, \mathcal{L} is the effective integrated luminosity and $\Phi = 0.0203$ is the effective photon flux as given by equation (1) after integration over the selected W and Q^2 ranges. The branching ratio of the $\omega \rightarrow \pi^+ \pi^- \pi^0$ ($\pi^0 \rightarrow \gamma\gamma$) decay is $B = B_{\omega \rightarrow 3\pi} \cdot B_{\pi^0 \rightarrow \gamma\gamma} = 0.877$ [17]. In the region of $|t| < 0.6 \text{ GeV}^2$, and averaged over the range $70 < W < 90 \text{ GeV}$, the cross section is:

$$\sigma_{\gamma p \rightarrow \omega p} = 1.21 \pm 0.12(\text{stat.}) \pm 0.23(\text{syst.}) \mu\text{b}.$$

The systematic error was obtained by adding in quadrature the individual contributions listed in Table 1; the dominant ones are from the acceptance calculation and the inelastic background subtraction.

The resulting elastic $\gamma p \rightarrow \omega p$ cross section at an average energy of $\langle W \rangle = 80 \text{ GeV}$ is shown in Figure 5 together with previous results from fixed target experiments [18]-[29]. The W dependence of the cross sections in the range $10 < W < 100 \text{ GeV}$ is found to be weak, as predicted by Regge fits to hadronic cross sections [30, 31].

As a consistency check, the elastic $\gamma p \rightarrow \phi p$ cross section was determined, using $B = B_{\phi \rightarrow 3\pi} \cdot B_{\pi^0 \rightarrow \gamma\gamma} = 0.154$ [17] and $\Phi = 0.0207$, resulting in $\sigma_{\gamma p \rightarrow \phi p} = 0.9 \pm 0.3(\text{stat.}) \mu\text{b}$. This value agrees with $\sigma_{\gamma p \rightarrow \phi p} = 0.96 \pm 0.19_{-0.18}^{+0.21} \mu\text{b}$ determined using the reaction $\gamma p \rightarrow \phi p$ ($\phi \rightarrow K^+ K^-$) in the kinematic range $60 < W < 80 \text{ GeV}$ and $|t| < 0.5 \text{ GeV}^2$ [5].

7.3 Differential cross section $d\sigma_{\gamma p \rightarrow \omega p}/d|t|$

In order to derive the differential cross section $d\sigma_{\gamma p \rightarrow \omega p}/d|t|$, the fit to the mass spectrum described in section 7.1 was repeated in bins of p_T^2 . To reconstruct the t distribution, a bin-by-bin correction [3], given by the ratio of the generated t and the reconstructed p_T^2 distribution in the PYTHIA Monte Carlo sample, was used to compensate for the difference between t and p_T^2 , which is a consequence of Q^2 not being measured. The result is shown in Figure 6(a). The data were fitted in the range $0 < |t| < 0.6 \text{ GeV}^2$ using the functional form:

$$\frac{d\sigma_{\gamma p \rightarrow \omega p}}{d|t|} = A \cdot e^{-b|t|}, \quad (4)$$

yielding:

$$\begin{aligned} A &= 10.7 \pm 2.2(\text{stat.}) \pm 2.3(\text{syst.}) \mu\text{b}/\text{GeV}^2, \\ b &= 10.0 \pm 1.2(\text{stat.}) \pm 1.3(\text{syst.}) \text{GeV}^{-2}. \end{aligned}$$

The systematic error in A is dominated by the uncertainty on the acceptance (sensitivity to cuts (16%) and model dependence (9%)); the other contributions are the inelastic background subtraction, radiative corrections and luminosity, as listed in Table 1. The dominant contribution to the systematic error in b is also the uncertainty on the acceptance (sensitivity to cuts (12%) and model dependence (4%)).

The slope b is compared in Figure 6(b) with the results of previous experiments [19, 20, 22, 24, 25, 28, 29]. From a study of diffractive hadronic processes, assumed to be mediated by Pomeron exchange, Regge theory gives the following dependence of the slope b on W (with W in GeV) [2]:

$$b = b_0 + 2\alpha'_{\text{P}} \ln W^2, \quad (5)$$

with $\alpha'_{\text{P}} = 0.25 \text{ GeV}^{-2}$. The line shown in Figure 6(b) represents the dependence according to equation (5), with b_0 chosen such that it passes through the ZEUS point. This behaviour is in good agreement with the data points at high energies ($W > 10 \text{ GeV}$), where equation (5) is expected to hold.

7.4 Decay angular distributions

The polar and azimuthal angles θ_h and ϕ_h of the normal to the ω meson decay plane in the s -channel helicity frame were used to determine elements of the ω spin-density matrix [32]. The direction of the normal was defined as that of $\vec{\pi}^+ \times \vec{\pi}^-$, where $\vec{\pi}^+$ ($\vec{\pi}^-$) is the three momentum of the positively (negatively) charged pion. The experimental resolution in $\cos\theta_h$ is about 0.05 and in ϕ_h about 0.8 rad. Upon averaging over ϕ_h or $\cos\theta_h$ one finds, respectively [32]:

$$\frac{1}{N} \frac{dN}{d\cos\theta_h} = \frac{3}{4} [1 - r_{00}^{04} + (3r_{00}^{04} - 1) \cos^2\theta_h], \quad (6)$$

$$\frac{1}{N} \frac{dN}{d\phi_h} = \frac{1}{2\pi} [1 - 2r_{1-1}^{04} \cos 2\phi_h]. \quad (7)$$

As the distribution of $\cos\theta_h$ was found to be symmetric, $|\cos\theta_h|$ was considered instead. The acceptance corrected distributions of $|\cos\theta_h|$ and ϕ_h are shown in Figure 7.

They were obtained by repeating the mass fits described in section 7.1, applied in each bin of $|\cos\theta_h|$ and ϕ_h . Fits of the functions (6) and (7) to the corrected data yield

$$r_{00}^{04} = 0.11 \pm 0.08(\text{stat.}) \pm 0.26(\text{syst.})$$

and

$$r_{1-1}^{04} = -0.04 \pm 0.08(\text{stat.}) \pm 0.12(\text{syst.}).$$

Both values are compatible with the prediction of s -channel helicity conservation: $r_{00}^{04} = 0.10$ (assuming a Q^2 dependence of the ratio of the longitudinal to the transverse γ^*p cross section from VDM as also used in equation (1)) and $r_{1-1}^{04} = 0$.

8 Comparison of elastic light vector meson photo-production measurements

In addition to the measurement presented above, elastic photoproduction of ρ^0 [3, 4] and ϕ [5] have also been measured at HERA. Table 2 gives a summary of the ZEUS results. The elastic ρ^0 cross section has also been measured by the H1 collaboration [4], who find a cross section of $9.1 \pm 0.9 \pm 2.5 \mu\text{b}$ at $\langle W \rangle = 55 \text{ GeV}$ and $13.6 \pm 0.8 \pm 2.4 \mu\text{b}$ at $\langle W \rangle = 187 \text{ GeV}$. We compare in the following our ρ^0 , ω and ϕ measurements with each other and with measurements at lower energy, which are presented in Table 3.

From the data of Tables 2 and 3 we calculated the ρ^0 to ω and ρ^0 to ϕ cross section ratios $\sigma_{\gamma p \rightarrow \rho^0 p} / \sigma_{\gamma p \rightarrow \omega p}$ and $\sigma_{\gamma p \rightarrow \rho^0 p} / \sigma_{\gamma p \rightarrow \phi p}$ for $\langle W \rangle = 12$ or 14 GeV and 70 or 80 GeV . The results are given in Table 4 and show no significant energy dependence, as expected if there is the same soft diffractive process mediated by Pomeron exchange for all three vector mesons.

Table 5 shows the energy dependence of ρ^0 , ω and ϕ elastic photoproduction cross sections, comparing data from this experiment at $\langle W \rangle = 70 \text{ GeV}$ or $\langle W \rangle = 80 \text{ GeV}$ with data from fixed target experiments from Table 3.

Using the optical theorem and VDM, the differential cross section $d\sigma_{\gamma p \rightarrow Vp} / d|t|$ for vector meson photoproduction, with $V = \rho^0$, ω or ϕ , can be related to the total vector meson proton cross section σ_{Vp} , assuming that the real part of the amplitude is zero:

$$\left. \frac{d\sigma_{\gamma p \rightarrow Vp}}{d|t|} \right|_{t=0} = \frac{4\pi\alpha}{f_V^2} \frac{1}{16\pi} \sigma_{Vp}^2, \quad (8)$$

where $f_V^2/4\pi$ is the vector meson photon coupling constant. Using equation (8) and the approximate relation:

$$\left. \frac{d\sigma_{\gamma p \rightarrow Vp}}{d|t|} \right|_{t=0} = b \cdot \sigma_{\gamma p \rightarrow Vp},$$

one finds:

$$\sigma_{\gamma p \rightarrow Vp} = \frac{4\pi\alpha}{16\pi f_V^2} \frac{1}{b} \sigma_{Vp}^2.$$

At these large energies, the total Vp cross sections are expected to increase with energy [35] proportionally to $W^{2\alpha_{\mathbb{P}}(0)-2}$, where $\alpha_{\mathbb{P}}(0)$ is the intercept of the Pomeron trajectory. With $\alpha_{\mathbb{P}}(0) = 1.08$ [31], and assuming the slope b to increase with W according to equation (5), one finds an increase in the elastic vector meson photoproduction cross sections with energy as shown in Table 5. The predictions are consistent with the data.

Equation (8) can be used to compute the total ω proton cross section. Using $\left. \frac{d\sigma}{d|t|} \right|_{t=0} = 10.7 \mu\text{b}/\text{GeV}^2$ (see Table 2) and $f_\omega^2/4\pi = 23.6$ [34], one gets

$$\sigma_{\omega p} = 26.0 \pm 2.5(\text{stat.})_{-4.2}^{+3.0}(\text{syst.}) \text{ mb},$$

where the systematic error includes the error of $\left. \frac{d\sigma}{d|t|} \right|_{t=0}$ and the estimated uncertainty of $f_\omega^2/4\pi$. This value agrees with the expected value of 28 mb at $W = 80 \text{ GeV}$, obtained from a parametrisation of $\sigma_{\omega p} = \frac{1}{2}(\sigma_{\pi^+p} + \sigma_{\pi^-p})$ [30].

9 Conclusions

Elastic ω photoproduction at $\langle W \rangle = 80 \text{ GeV}$ and $|t| < 0.6 \text{ GeV}^2$ has been measured using the ZEUS detector. The elastic cross section is $\sigma_{\gamma p \rightarrow \omega p} = 1.21 \pm 0.12 \pm 0.23 \mu\text{b}$. The exponential slope of the differential cross section $d\sigma_{\gamma p \rightarrow \omega p}/d|t|$ in this t range has been determined to be $10.0 \pm 1.2 \pm 1.3 \text{ GeV}^{-2}$. The angular distributions of the decay pions are consistent with s -channel helicity conservation.

A comparison of light vector meson photoproduction as measured by ZEUS with measurements at lower centre-of-mass energies ($\langle W \rangle \approx 14 \text{ GeV}$) is consistent with no energy dependence of the ρ^0 to ω and ρ^0 to ϕ cross section ratios. All these results are consistent with the photoproduction of light vector mesons being dominated by a soft diffractive process.

10 Acknowledgement

We thank the DESY Directorate for their strong support and encouragement. The remarkable achievements of the HERA machine group were essential for the successful completion of this work and are gratefully appreciated.

For the design and construction of the RHES special thanks go to D. Cassel, S. Kasai, A. Montag, K.U. Pösnecker, V. Radeka and R. Rau, who contributed in the early stage of the project. The engineering and technical support of the following institutes is gratefully acknowledged: Faculty of Physics and Nuclear Techniques, Cracow; DESY; Univ. of Hamburg; Univ. Autónoma Madrid; Moscow State Univ.; Univ. of Tokyo and Weizmann Institute.

References

- [1] J.J. Sakurai, Ann. Phys. **11** (1960) 1;
J.J. Sakurai, Phys. Rev. Lett. **22** (1969) 981.
- [2] P.D.B. Collins, *An Introduction to Regge Theory and High Energy Physics*,
Cambridge University Press (1977).
- [3] ZEUS Collab., M. Derrick et al., Z. Phys. **C69** (1995) 39.
- [4] H1 Collab., S. Aid et al., Nucl. Phys. **B463** (1996) 3.
- [5] ZEUS Collab., M. Derrick et al., Phys. Lett. **B377** (1996) 259.
- [6] The ZEUS Detector, Status Report, DESY (1993).
- [7] C. Alvisi et al., Nucl. Instrum. Methods **A 305** (1991) 30.
- [8] N. Harnew et al., Nucl. Instrum. Methods **A 279** (1989) 290;
C.B. Brooks et al., Nucl. Instrum. Methods **A 283** (1989) 477;
B. Foster et al., Nucl. Instrum. Methods **A 338** (1994) 254.
- [9] B. Bock et al., Nucl. Instrum. Methods **A 344** (1994) 335.
- [10] M. Derrick et al., Nucl. Instrum. Methods **A 309** (1991) 77;
A. Andresen et al., Nucl. Instrum. Methods **A 309** (1991) 101;
A. Bernstein et al., Nucl. Instrum. Methods **A 336** (1993) 23.

- [11] A. Dwurażny et al., Nucl. Instrum. Methods **A 277** (1989) 176.
- [12] W.H. Smith et al., Nucl. Instrum. Methods **A 355** (1995) 278.
- [13] T. Sjöstrand and M. Bengtsson, Comput. Phys. Commun. **43** (1987) 367;
M. Bengtsson and T. Sjöstrand, Comput. Phys. Commun. **46** (1987) 43;
T. Sjöstrand, in “Proceedings of the Workshop Physics at HERA”, DESY, 29-30
October 1991, ed. W. Buchmüller and G. Ingelman, p. 1405.
- [14] M. Arneodo, L. Lamberti and M.G. Ryskin, submitted to Comput. Phys. Com-
mun.
- [15] H. Abramowicz et al., Phys. Lett. **B269** (1991) 465.
- [16] M.G. Ryskin, Z. Phys. **C 57** (1993) 89.
- [17] R.M. Barnett et al., Phys. Rev. **D54** (1996) 1.
- [18] H.R. Crouch et al., Phys. Rev. **155** (1967) 1468.
- [19] ABBHHM Collab., R. Erbe et al., Phys. Rev. **175** (1968) 1669.
- [20] M. Davier et al., Phys. Rev. **D1** (1970) 790.
- [21] SWT Collab., Y. Eisenberg et al., Phys. Rev. **D5** (1972) 15.
- [22] SBT Collab., J. Ballam et al., Phys. Rev. **D7** (1973) 3150.
- [23] W. Struczinski et al., Nucl. Phys. **B108** (1976) 45.
- [24] R.M. Egloff et al., Phys. Rev. Lett. **43** (1979) 1545 and **44** (1980) 690 (Erratum).
- [25] A.M. Breakstone et al., Phys. Rev. Lett. **47** (1981) 1782.
- [26] D. Aston et al., Nucl. Phys. **B209** (1982) 56.
- [27] LAMP2 Group, D.P. Barber et al., Z. Phys. **C26** (1984) 343.
- [28] OMEGA Collab., M. Atkinson et al., Nucl. Phys. **B231** (1984) 15.
- [29] J. Busenitz et al., Phys. Rev. **D40** (1989) 1.
- [30] G.A. Schuler and T. Sjöstrand, Nucl. Phys. **B407** (1993) 539.

- [31] A. Donnachie and P.V. Landshoff, Nucl. Phys. **B231** (1984) 189.
- [32] K. Schilling, P. Seyboth and G. Wolf, Nucl. Phys. **B15** (1970) 397;
K. Schilling and G. Wolf, Nucl. Phys. **B61** (1973) 381.
- [33] R.M. Egloff et al., Phys. Rev. Lett. **43** (1979) 657.
- [34] T.H. Bauer et al., Rev. Mod. Phys. **50** (1978) 261.
- [35] H. Cheng, J.K. Walker and T.T. Wu, Phys. Lett. **B44** (1973) 97.

Source	Error [%]	Refer to
Luminosity	1.5	
Acceptance: <ul style="list-style-type: none"> • sensitivity to track selection cuts (modify to $p_T > 150 \text{ MeV}$ or $\theta < 163^\circ$ or $\theta < 167^\circ$); • sensitivity to RCAL and RHES energy cuts (change by 50% or assume a miscalibration of RHES by 20%); • sensitivity to $M_{\gamma\gamma}$ range (change cut on $M_{\gamma\gamma} - \langle M_{\gamma\gamma} \rangle$ by $\pm 10 \text{ MeV}$); • sensitivity to W range (change cut values by 6%); • trigger efficiency; • model dependence. 	4	Section 4.1
	8	Section 4.2
	9	Section 4.2
	5	Section 4.3
	6	Section 5
	3	Section 5
Radiative corrections	4	Section 5
Inelastic background subtraction	11	Section 6
Total (added in quadrature)	19	

Table 1: Contributions to the systematic error on $\sigma_{\gamma p \rightarrow \omega p}$.

	$\gamma p \rightarrow \rho^0 p$	$\gamma p \rightarrow \omega p$	$\gamma p \rightarrow \phi p$
$\langle W \rangle$ [GeV]	70	80	70
σ [μb]	$14.7 \pm 0.4 \pm 2.4$	$1.21 \pm 0.12 \pm 0.23$	$0.96 \pm 0.19_{-0.18}^{+0.21}$
$ t $ -range [GeV^2]	< 0.5	< 0.6	< 0.5
$\frac{d\sigma}{d t } _{t=0}$ [$\mu\text{b}/\text{GeV}^2$]	$139 \pm 6 \pm 26$	$10.7 \pm 2.2 \pm 2.3$	$7.2 \pm 2.1 \pm 1.5$
b [GeV^{-2}]	$10.4 \pm 0.6 \pm 1.1$	$10.0 \pm 1.2 \pm 1.3$	$7.3 \pm 1.0 \pm 0.8$
$ t $ -range [GeV^2]	< 0.15	< 0.6	$0.1 < t < 0.5$
ref.	[3]	this paper	[5]

Table 2: Summary of results on elastic light vector meson photoproduction at HERA as measured by ZEUS in the given t range. The values of $\frac{d\sigma}{d|t|}|_{t=0}$ and of b have been taken from a fit of the differential cross section of the form $\frac{d\sigma}{d|t|} = \frac{d\sigma}{d|t|}|_{t=0} \cdot e^{-b|t|}$ in the given t range.

	$\gamma p \rightarrow \rho^0 p$	$\gamma p \rightarrow \omega p$	$\gamma p \rightarrow \phi p$
$\langle W \rangle$ [GeV]	12	14	14
σ [μb]	9.25 ± 0.44	1.07 ± 0.12	0.66 ± 0.08
ref.	[26, 33]	[24, 25, 28, 29]	[33]

Table 3: Elastic $\gamma p \rightarrow Vp$ cross sections from fixed target experiments for $W \geq 9$ GeV. The values listed were obtained as weighted means of the cited measurements.

$\langle W \rangle$	$\sigma_{\gamma p \rightarrow \rho^0 p} / \sigma_{\gamma p \rightarrow \omega p}$	$\sigma_{\gamma p \rightarrow \rho^0 p} / \sigma_{\gamma p \rightarrow \phi p}$
12 or 14 GeV	8.6 ± 1.0	14.0 ± 1.8
70 or 80 GeV	12.2 ± 3.0	15.3 ± 4.9

Table 4: Ratios of vector meson photoproduction cross sections.

	$\frac{\sigma_{\gamma p \rightarrow \rho^0 p}^{\langle W \rangle=70}}{\sigma_{\gamma p \rightarrow \rho^0 p}^{\langle W \rangle=12}}$	$\frac{\sigma_{\gamma p \rightarrow \omega p}^{\langle W \rangle=80}}{\sigma_{\gamma p \rightarrow \omega p}^{\langle W \rangle=14}}$	$\frac{\sigma_{\gamma p \rightarrow \phi p}^{\langle W \rangle=70}}{\sigma_{\gamma p \rightarrow \phi p}^{\langle W \rangle=14}}$
Experiment	1.59 ± 0.28	1.12 ± 0.22	1.45 ± 0.46
Pomeron exchange	1.46	1.45	1.28
b_0 (from eq. (5))	6.15	5.75	3.05

Table 5: Ratio of cross sections at high and low W .

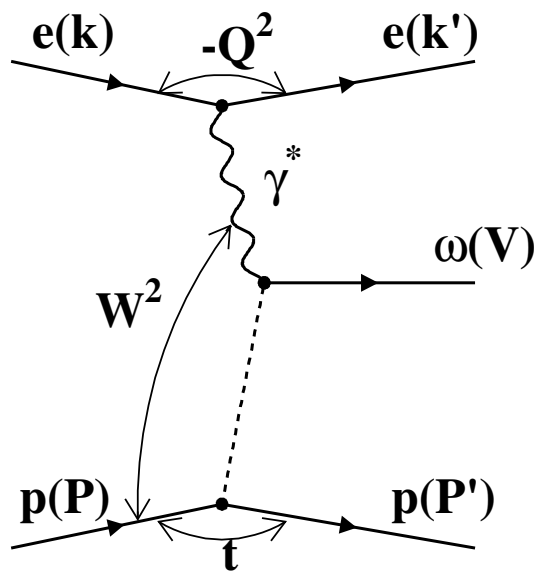


Figure 1: Schematic diagram of elastic ω production in ep interactions.

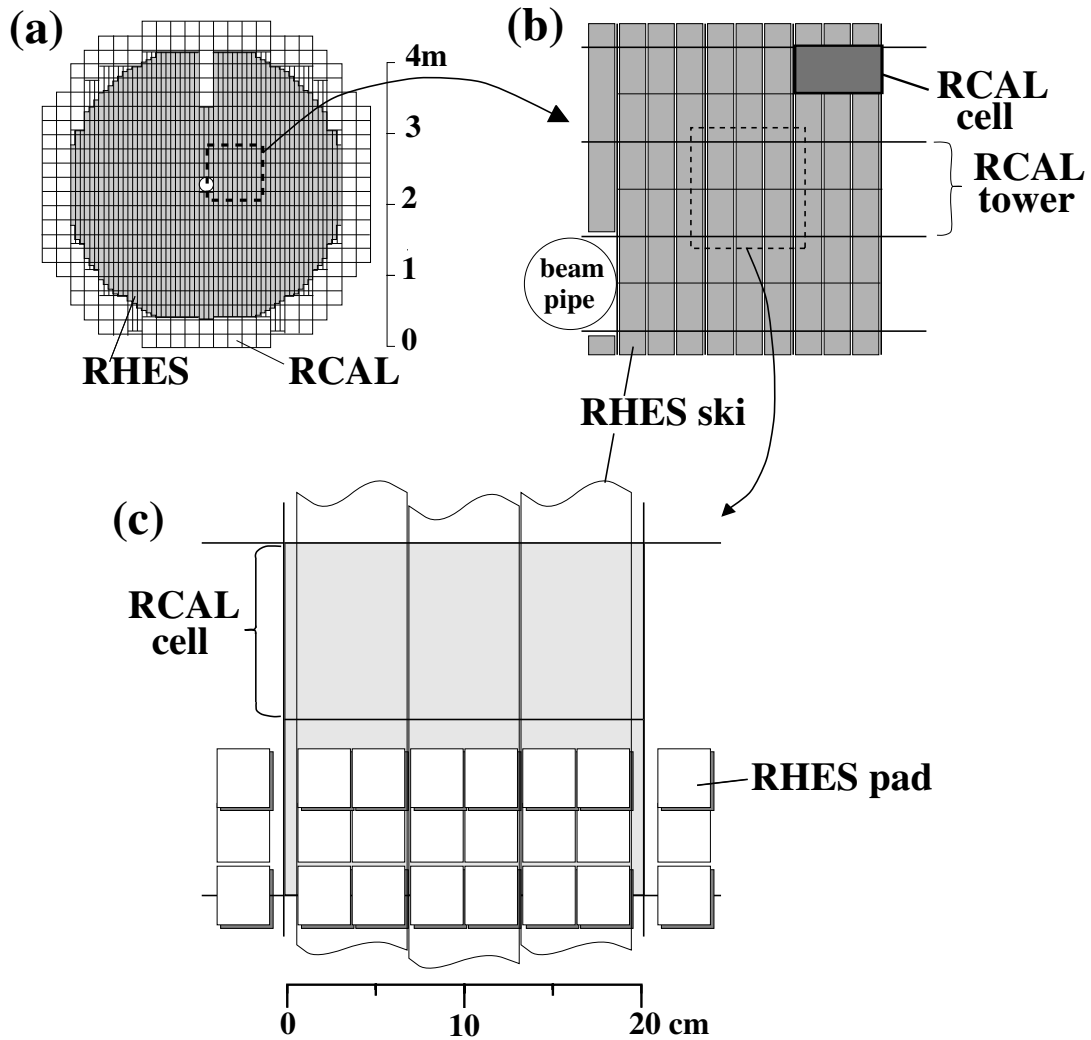


Figure 2: (a) The area covered by RHES in the RCAL as seen from the interaction point. (b) Extended view of (a), indicating the division of the RCAL EMC into modules and towers. Two RCAL EMC cells fit into one tower. The RHES pads are mounted on support structures, called skis in the figures. (c) Extended view of an RCAL tower. The segmentation of RHES into the pads is shown. 6×3 pads fit into one RCAL EMC cell.

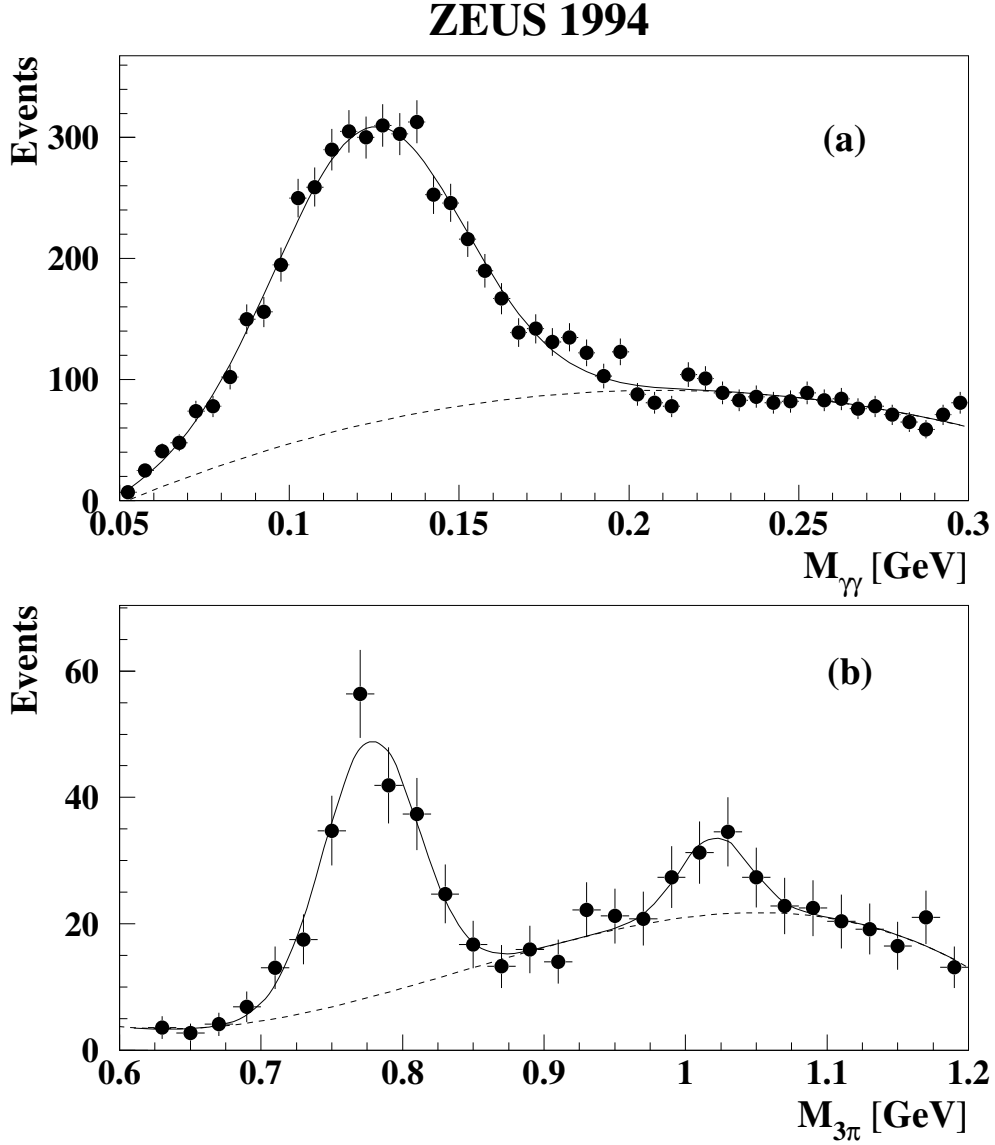


Figure 3: (a) Invariant mass distribution of the two photons. The full line is the result of the fit explained in the text. (b) Invariant mass distribution of the $\pi^+\pi^-\pi^0$ system after all offline cuts and the fit based on equation (2). The full line is a fit based on equation (3). In both figures the dashed line indicates the background as determined by the fits.

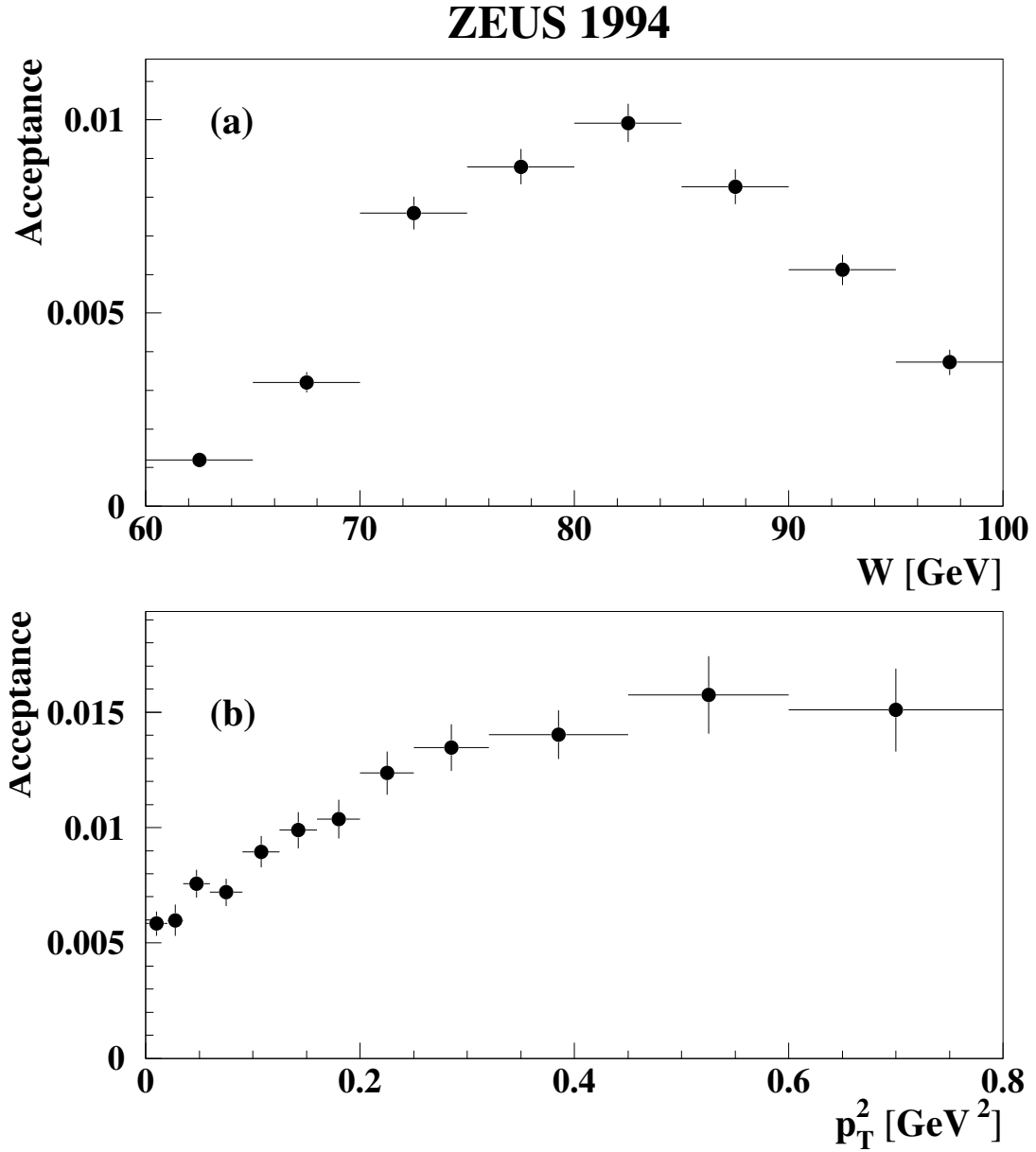


Figure 4: Acceptance for the process $ep \rightarrow ewp$. (a) Acceptance as a function of W in the range $|t| < 0.6 \text{ GeV}^2$. (b) Acceptance as a function of p_T^2 in the range $70 < W < 90 \text{ GeV}$.

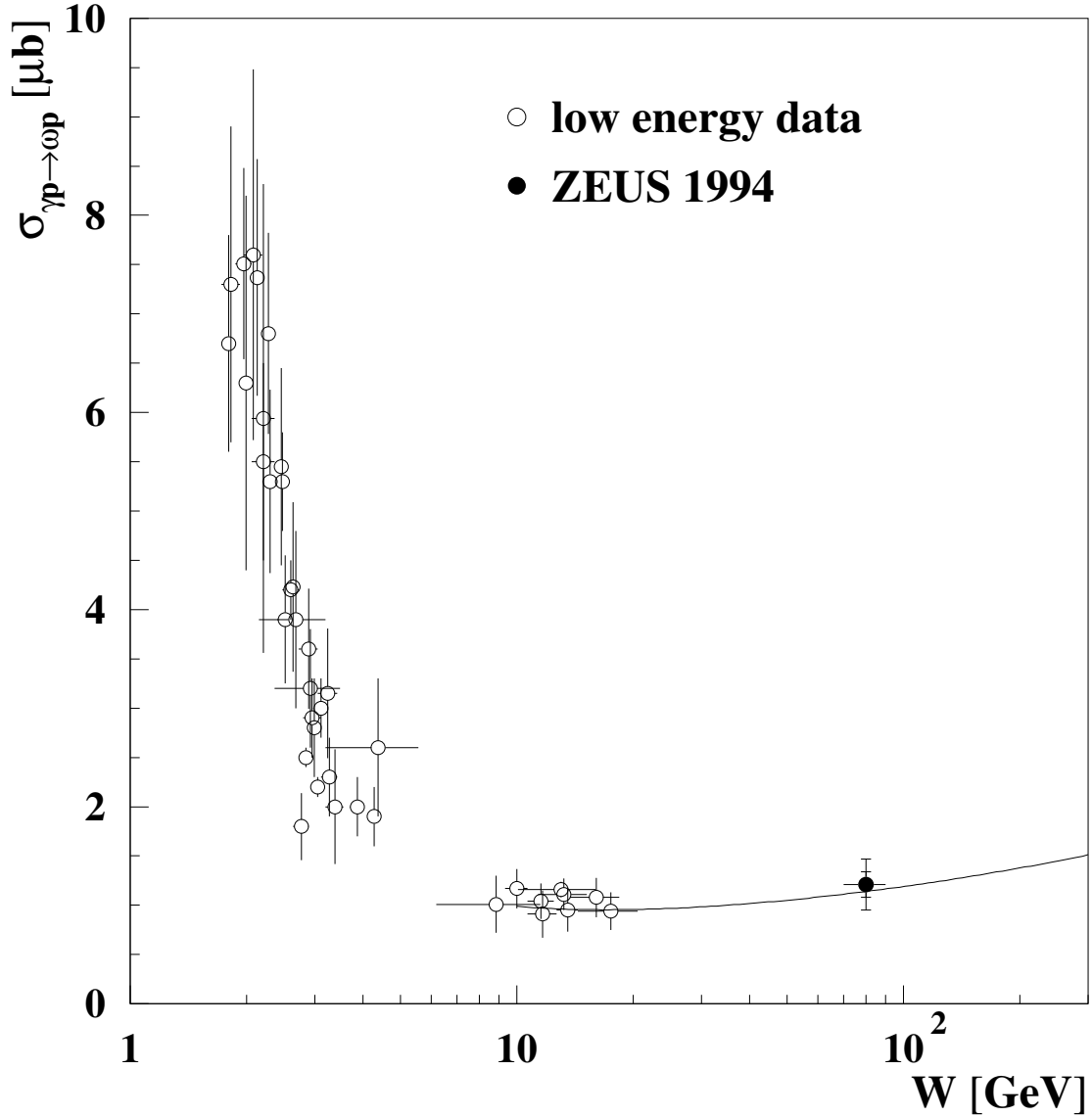


Figure 5: The elastic $\gamma p \rightarrow \omega p$ cross section measured in this experiment (solid circle) compared with the results of fixed target experiments [18]-[29] (open circles). For the ZEUS measurement the inner part of the vertical error bar shows the statistical error, while the outer one shows the statistical and systematic errors added in quadrature. The horizontal bars indicate the W range covered by the measurements. The line is a parametrisation based on Regge fits to hadronic data [30].

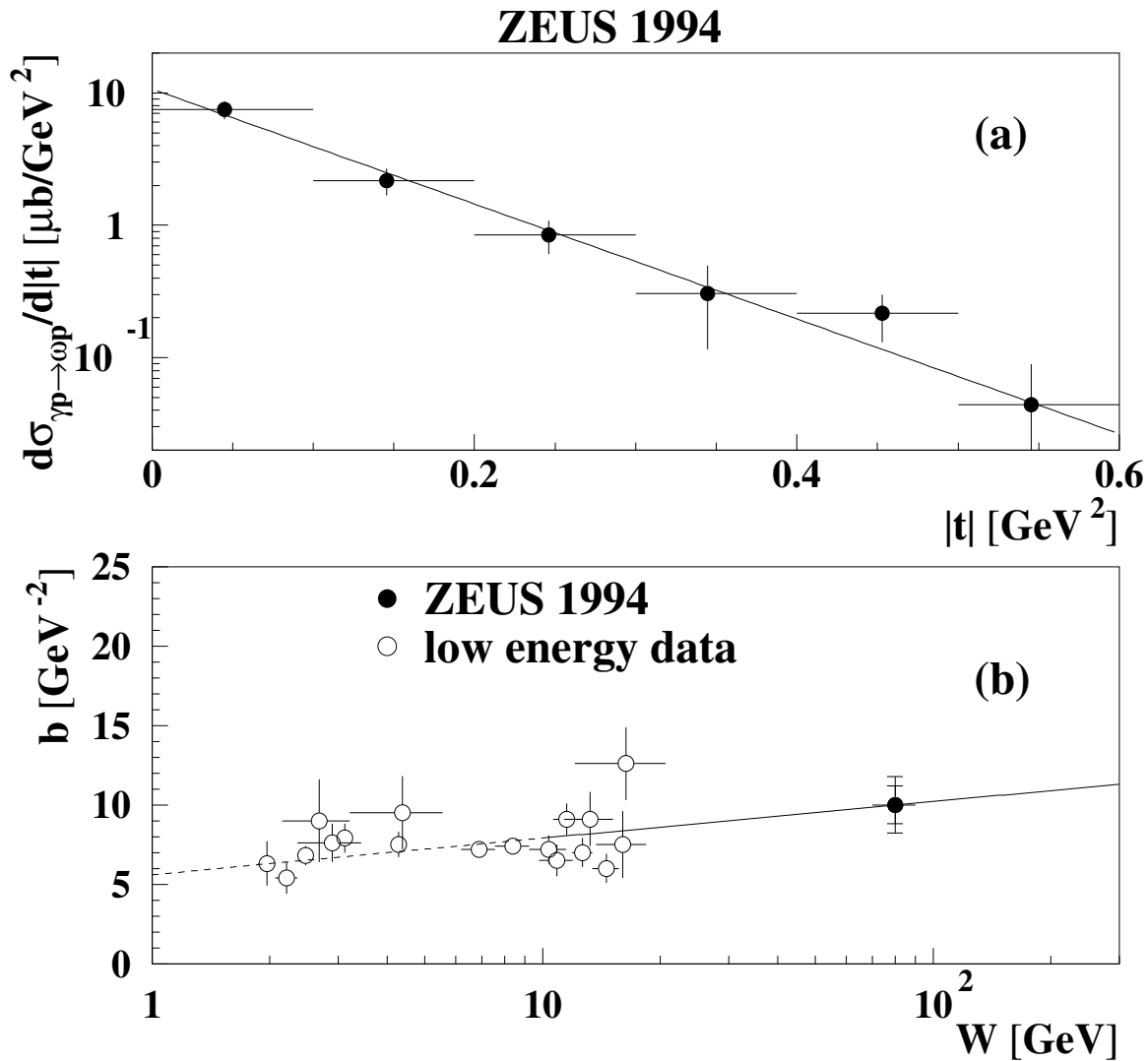


Figure 6: (a) The differential cross section $d\sigma_{\gamma p \rightarrow \omega p}/d|t|$; the line shows the result of the fit with functional form (4). (b) Exponential slope b of $d\sigma_{\gamma p \rightarrow \omega p}/d|t|$ as observed in this experiment (solid circle) compared with low energy data [19, 20, 22, 24, 25, 28, 29] (open circles). For the ZEUS measurements the inner part of the vertical error bar shows the statistical error, while the outer one shows the statistical and systematic errors added in quadrature. The horizontal bars indicate the W range covered by the measurements. The line is given by equation (5). It was constrained to pass through the ZEUS data point.

ZEUS 1994

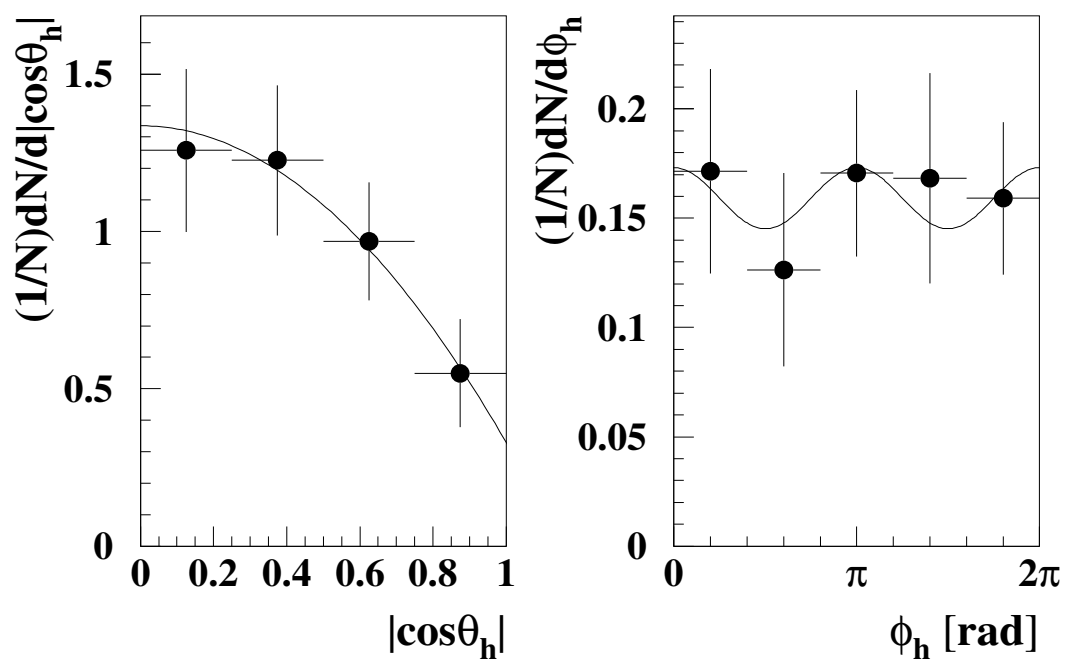


Figure 7: Acceptance corrected distribution of $|\cos\theta_h|$ and ϕ_h , where θ_h and ϕ_h are the polar and azimuthal angles of the ω meson decay plane in the s -channel helicity frame, respectively. Fits according to equations (6) and (7) are superimposed.